Characterization of Poly(vinyl alcohol)/Gold Nanocomposites Obtained by *In Situ* Gamma-Irradiation Method

Aleksandra Radosavljević, Dušan Božanić, Nataša Bibić, Miodrag Mitrić, Zorica Kačarević-Popović, Jovan Nedeljković

Vinča Institute of Nuclear Sciences, University of Belgrade, Belgrade 11001, Serbia

Received 6 April 2011; accepted 27 May 2011
DOI 10.1002/app.34992
Published online 7 January 2012 in Wiley Online Library (wileyonlinelibrary.com).

ABSTRACT: Gamma-irradiation induced reduction of gold (Au) ions was performed in aqueous poly(vinyl alcohol) (PVA) solution. PVA/Au nanocomposites with different contents of inorganic phase were prepared by solvent evaporation. The colloids and corresponding nanocomposites show visible light absorption with strong excitonic peak in the wavelength range from 520 to 550 nm. Morphological and structural characterizations of gold nanoparticles (Au NPs) and nanocomposites were performed by TEM, XRD, and FTIR measurements. Also, Mie and Maxwell-Garnett theories were applied to calculate optical properties of Au colloids and PVA/Au nanocomposites, respectively. The changes of heat resistance upon the increase of inorganic phase were correlated to the decrease in crystal perfection of polymer. Improvement of thermal stability of nanocomposites, compared with the neat PVA, was observed when the content of inorganic phase exceeds 1 wt %. © 2012 Wiley Periodicals, Inc. J Appl Polym Sci 125: 1244–1251, 2012

Key words: Gamma-irradiation; Au nanoparticles; PVA/Au nanocomposites; optical properties; thermal properties

INTRODUCTION

Nanotechnology is one of the fastest growing new areas in science and engineering. Polymers are considered to be a good host material for incorporation of inorganic nanoparticles (NPs). On the other hand, incorporation of inorganic NPs, due to their high surface to bulk ratio, can significantly affect the properties of the polymer matrix. Organic polymers containing metal NPs are considered to be functional composite materials.

Noble metal NPs are of great significance due to their optical properties which are the consequence of the electromagnetic field induced collective oscillations of electrons known as surface plasmon resonance (SPR).[1,2] Existence of plasmon modes rise strong absorption in UV-vis region. The number, shape, and position of plasmon absorption bands in absorption spectrum of noble metal NPs are determined by particle size, shape, dielectric constant, composition, and dielectric constant of the surrounding media.[3,4]

Among a number of techniques reported for the synthesis of Au NPs, the radiation induced synthesis is one of the most promising strategies due to several advantages compared with conventional chemical and photochemical methods.[5–8] Au NPs can be used in biological application such as DNA sensors,[9] drug delivery,[10] cancer diagnostic and therapy,[11] and therefore preparation of a biocompatible and nontoxic system containing Au NPs is a challenging task. Although chemical methods for the preparation of Au NPs have been widely used, reducing and/or stabilizing agents might be associated with environmental toxicity or biological hazards. These disadvantages can be overcome by using radiolytic method of synthesis.

The radiolytic method is particularly suitable for generation of metal NPs in solution, because the radiolytically generated species exhibit strong reducing power and reduction of metal ions occur at each encounter. However, metal atoms formed this way tend to coalesce into clusters, which grow into particles or eventually into precipitates. The control of particle size can be achieved by the use of capping agents such as polymers. Functional groups of polymers with a high affinity for the metal ensure the anchoring of the molecule at the particle surface, while the polymeric chains protect particles from coalescing with other ones, and thus inhibit at an early stage further coalescence through electrostatic repulsion or steric hindrance. Some of these polymeric systems can be, at the same time, the stabilizer and the reducing agent.[12,13] Poly(vinyl alcohol) (PVA) has been widely used as a matrix for preparation of

Correspondence to: A. Radosavljević (Krklješ) (krkljes@vinca.rs).

Contract grant sponsor: Ministry of Education and Science of the Republic of Serbia; contract grant number: 45020.

nanocomposites due to its easy processability, high optical clarity, and biocompatibility.[14]

In this work, the PVA/Au nanocomposites were prepared by the simple radiolytic procedure using steady state gamma-irradiation followed by solvent evaporation. The aim of this study was to explore the applicability of radiation technique for the synthesis of PVA/Au nanocomposites, as well as investigation of their optical and structural properties. Special attention was paid to the understanding of interaction between polymer chains and Au NPs and its influence on the heat resistance and thermal stability of the nanocomposites.

EXPERIMENTAL

All chemicals were of analytical grade and they were used without additional purification. Hydrogen tetrachloroaurate(III) ($HAuCl_4$), with min. 49% of Au, was obtained from Alfa Aesar. PVA with $M_w = 72{,}000$ and 99% of minimal degree of hydrolysis and 2-propanol were product of Merck. Water used in experiments was distilled and then purified using a Milli-Q Water System from Milipore Corps. High purity argon gas (99.5%) was from Messer Tehnogas.

$HAuCl_4$ was dissolved in water solutions containing 1.4 wt % PVA and 0.2 *M* 2-propanol. Concentrations of $HAuCl_4$ were 0.15, 0.29, 0.59, 1.47, 2.94, and 4.71 m*M*. The solutions were bubbled with Ar for about 30 min to remove oxygen, and then irradiated in ^{60}Co radiation facility at room temperature with irradiation dose rate of 10 kGy/h. Integral absorbed doses required for complete reduction of gold ions were 0.7, 1.4, 2.8, 6.9, 13.8, and 22 kGy, respectively. PVA/Au nanocomposites were obtained after solvent evaporation at room temperature.

The content of Au NPs in nanocomposites was determined by atomic absorption spectroscopy using Philips-Pyu Unicam SP 9 AAS spectrophotometer. The contents of inorganic phase in the nanocomposites were found to be 0.25, 0.6, 1.0, 2.5, 5.3, and 8.0 wt %.

Transmission electron microscopy (TEM) measurements were performed using Philips EM 400 microscope operated at an accelerating voltage of 120 kV. Samples for TEM studies were prepared by placing a drop of the colloidal dispersion of Au NPs onto a C-coated Cu grid. The size distribution of Au NPs was determined taking into account the diameters of about 450 particles.

The X-ray diffraction (XRD) measurements of the PVA/Au nanocomposites were performed on Bruker D8 Advance Diffractometer.

Absorption spectra of Au colloids and corresponding PVA/Au nanocomposites were recorded using Perkin–Elmer Lambda 5 spectrophotometer.

FTIR spectra of neat PVA and PVA/Au nanocomposites were recorded using Thermo Electron Corp. Nicolet 380 FTIR Spectrophotometer with ATR (Attenuated Total Reflection) accessory, equipped with a diamond tip.

Differential scanning calorimetric (DSC) analysis of PVA and PVA/Au nanocomposites was performed on SETARAM DSC 151R system under nitrogen atmosphere (flow rate 30 mL/min). The samples weighting about 7 mg were heated from 30 to 240°C, at the heating rate 10°C/min.

Thermogravimetric measurements were carried out using a SETSYS Evolution 1750 Thermogravimetry Analyzer in argon atmosphere (flow rate 20 mL/min) from 30 to 600°C (heating rate 10°C/min).

RESULTS AND DISCUSSION

The ionic species of noble metals can be reduced by exposing their aqueous solutions to γ-irradiation. The absorption of radiation energy occurs in the solvent and primary products of water radiolysis are shown in eq. (1)[15]:

$$H_2O \rightsquigarrow e^-_{aq}(2.7), OH^\bullet(2.7), H^\bullet(0.6), H_2(0.45), H_2O_2(0.7) \quad (1)$$

The numbers in parenthesis represents the respective *G* values. The *G* values for a given irradiated system are the absolute chemical yield expressed as the number of individual chemical events occurring per 100 eV of absorbed energy. The solvated electron (e^-_{aq}) and hydrogen atom ($H^\bullet$) are strong reducing agents, while the hydroxyl radical ($OH^\bullet$) is strong oxidizing agent. Because of that, $OH^\bullet$ radical scavenger (2-propanol) is added in the solution. It is well known that in the presence of alcohol, the $OH^\bullet$ and $H^\bullet$ radical species abstract hydrogen from the alcohols to produce an alcohol radical. Also, PVA can compete for $OH^\bullet$ radicals forming polymeric $PVA^\bullet$ radicals. To conclude, under given experimental conditions, three different reducing species (solvated electrons, 2-propanol and $PVA^\bullet$ radicals) with different reducing ability, formed by γ-irradiation, simultaneously induced the reduction of ionic gold species forming stable wine-red transparent colloidal solution consisting of Au NPs. The role of PVA was also to stabilize Au NPs and protect them from further growth.

The shape and size distribution of the Au NPs were examined by TEM. Typical TEM micrograph of Au NPs is presented in Figure 1(a). The presence of spherical nonagglomerated Au NPs can be clearly seen. The thorough particle sizing confirmed the presence of Au particles in the size range from 2 to 12 nm, with average diameter of 5.7 nm [Fig. 1(b)].

The X-ray diffraction pattern of Au NPs incorporated in PVA matrix is shown in Figure 2. The

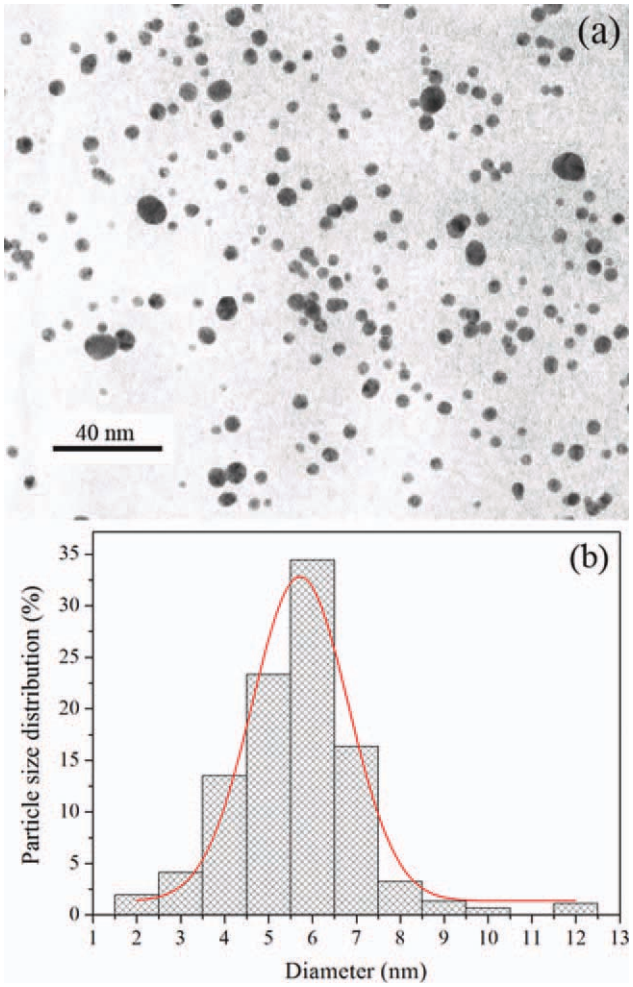

Figure 1 Typical TEM micrograph (a) and size distribution (b) of Au NPs. [Color figure can be viewed in the online issue, which is available at wileyonlinelibrary.com.]

prominent peaks at 2θ values of about 38.1, 44.3, 64.4, 77.4, and 81.6 degrees represent the, (111), (200), (220) (311), and (222) Bragg reflections from crystal planes of face centered cubic structure of gold.[16] The Sherrer diffraction formula was used to estimate the crystalline domain size (d):

$$d = \frac{k\lambda}{\beta \cos \theta} \tag{2}$$

where k is a constant for cubic structure (0.9), λ is the X-ray wavelength (0.1541 nm), β is the peak angular half-width and θ is the diffraction angle. The crystalline domain size was found to be 6.3 nm, which is in a good agreement with average diameter of Au NPs estimated by TEM.

The UV-vis absorption spectra of colloidal gold and the corresponding PVA/Au nanocomposite are presented in Figure 3 (black and red solid curves, respectively). The photographs of colloid and nanocomposite are presented as inset to Figure 3(a,b, respectively). It can be seen that the gold colloid exhibits surface plasmon resonance (SPR) band with a maximum at 523 nm. The peak position does not change in the entire concentration range, while the intensity is proportional to the concentration of Au NPs (not shown). Red shift of SPR band was observed after water evaporation and formation of nanocomposites. In the case of nanocomposite with the highest content of Au NPs (8 wt %) red shift of about 24 nm was observed. To exclude the possibility that observed changes are consequence of agglomeration of Au NPs upon formation of nanocomposite, transparent PVA/Au nanocomposite film was dissolved in water and absorption spectrum (Fig. 3, blue solid curve) was compared with the initial absorption spectrum of colloidal gold (Fig. 3, black solid curve). Absorption spectrum of the dissolved nanocomposite has SPR band at 527 nm, and it is almost identical to the absorption spectrum of primary gold colloid indicating that observed optical changes are not the consequence of agglomeration.

To gain further insight into the morphology of the investigated systems, the theoretical absorption spectra of gold colloid and PVA/Au nanocomposite films were calculated using Mie[17] and Maxwell-Garnett[18] theory, respectively. The theoretical curves were calculated using the experimental values for the complex dielectric function of gold[19] corrected for particle size.[20] Calculated spectrum obtained using Mie theory for single 6 nm golden spheres[2,7,17] is in a good agreement with the experimental spectrum of Au colloid (compare black solid and dashed curves in Fig. 3). In the case of PVA/Au nanocomposite, the red shift is expected due to the increase of the refractive index of the surrounding media[1,4] (1.33 and 1.53 for water and PVA, respectively,[21]). However, the change of dielectric environment of

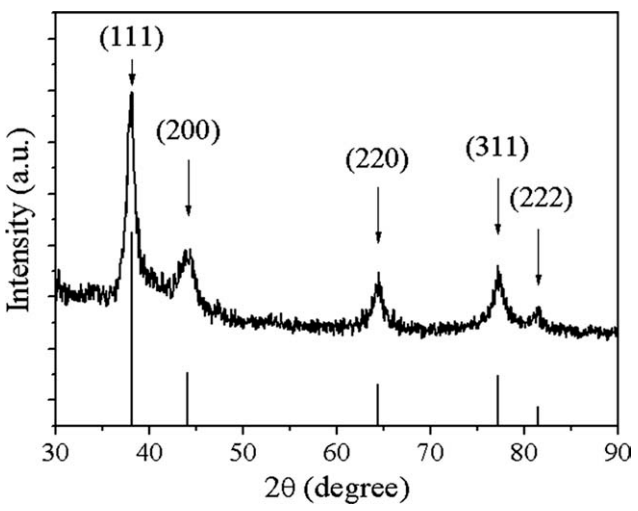

Figure 2 The XRD pattern of PVA/Au nanocomposite with 2.5 wt % of inorganic phase.

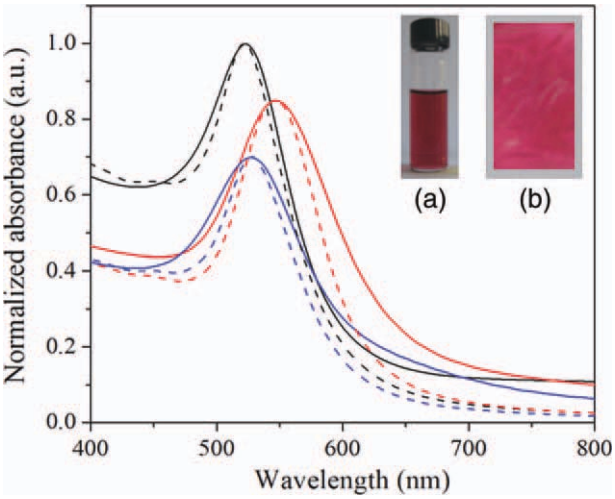

Figure 3 UV-Vis absorption spectra of Au colloid (black solid curve), the corresponding PVA/Au (92/8) nanocomposite film (red solid curve) and dissolved PVA/Au nanocomposite (blue solid curve). Theoretical absorption bands for Au NPs in water calculated using Mie theory (black dashed curve), PVA/Au nanocomposite film calculated using Maxwell-Garnett theory (red dashed curve), and Au NPs in water coated with 1.5 nm thick PVA layer using Mie theory for core-shell nanoparticles (blue dashed curve). Inset: photographs of Au colloid (a) and corresponding PVA/Au nanocomposite obtained after water evaporation (b). [Color figure can be viewed in the online issue, which is available at wileyonlinelibrary.com.]

the NPs was not sufficient to explain the observed shift of 24 nm, since the Mie theory does not take into account any interaction between the particles. Therefore, the peak positions in the absorption spectra of the PVA/Au nanocomposite was reconstructed using effective medium Maxwell-Garnett theory[18] (Fig. 3, red dashed curve). In the theory, the occurrence of the metallic phase is described by the value of filling factor f, and for the PVA/Au nanocomposite the main contribution to the experimental spectrum arises for nanocomposite configuration with filling factor $f = 0.15$.

As already mentioned, the absorption spectra of initial gold colloid and dissolved PVA/Au nanocomposite are very similar (compare black and blue solid curves in Fig. 3). The only difference in absorption spectra is red shift of the dissolved nanocomposite for about 4 nm. To explain this small change of the SPR band position, the calculation based on extension of Mie theory for NPs capped with the thin dielectric layer was employed.[4] When the metal NP is capped with a thin dielectric layer, it induces perturbation which shifts the SPR band toward higher wavelengths.[22] The wavelength of SPR band of coated NP (λ_c^s), can be estimated using following equation[23]:

$$\lambda_c^s = \frac{hc}{\omega_p}\sqrt{\varepsilon_\infty + 2n_{\mathrm{H_2O}}^2 + \frac{2}{3}g\left(n_{\mathrm{PVA}}^2 - n_{\mathrm{H_2O}}^2\right)} \qquad (3)$$

where $\omega_p = 8.95$ eV is the bulk plasmon frequency, $\varepsilon_\infty = 1 + \mathrm{Re}\ \chi^{ib} = 9.5$ is the contribution of the vacuum and interband electronic transitions, n_{H_2O} and n_{PVA} are refractive indices of medium (water) and shell (PVA), respectively, and $g = 1 - (r/R)^3$ is the volume fraction of the shell layer ($R = r + d$ is the radius of the coated particle where d is the thickness of the layer). According to the extended Mie theory, observed position of SPR band indicates that the Au NPs are coated with approximately 1.5 nm thick PVA layer after the nanocomposite dissolution.

These results reveal that formation of nanocomposite by water evaporation did not induce the agglomeration or growth of Au NPs. In general, the thin shell polymer layer is formed due to polymer adsorption onto NP surface. Polymer adsorption onto surfaces is dominated by a balance between the chain conformational entropy which favors formation of thick layers, and the polymer-substrate interactions which favors adsorption in a flat configuration with many contact points. Polymer adsorption suppresses particle–particle aggregation by saturating the surface reactive sites and creating a protective layer, and it is govern by a balance between the adsorption energy per monomer at contact with the metal surface, the polymer-solvent mixing energy and the configurational entropy loss due to chain confinement on the surface.[24]

To investigate the origin of interaction between Au nanofiller and PVA matrix, FTIR measurements of neat PVA and PVA/Au nanocomposites were compared (Fig. 4). Decrease and complete disappearance of the band positioned at 1270 cm^{-1}, which correspond to the O—H in-plane vibrations was observed upon the increase of the content of inorganic phase.[25] Another change in the FTIR spectrum of the PVA/Au nanocomposites was observed for

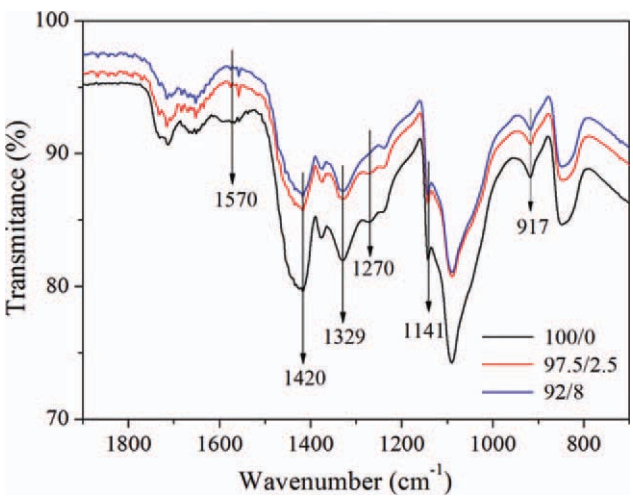

Figure 4 FTIR spectra of neat PVA and PVA/Au nanocomposite. [Color figure can be viewed in the online issue, which is available at wileyonlinelibrary.com.]

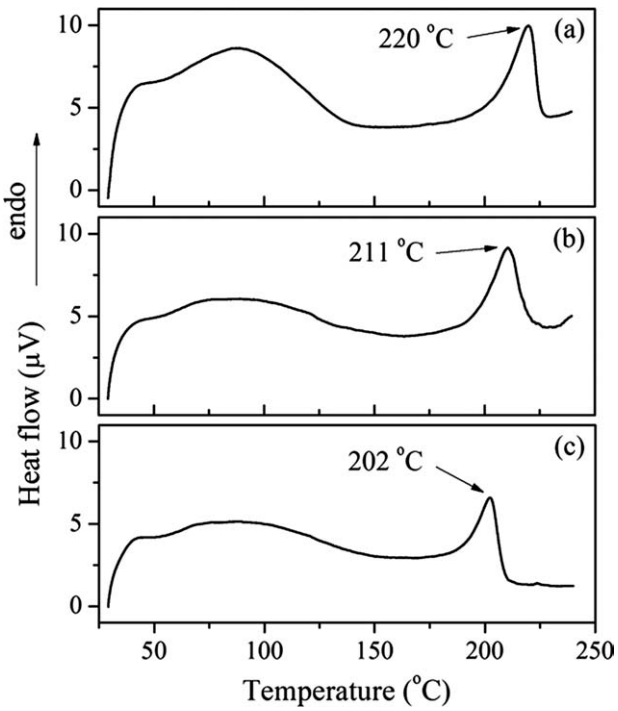

Figure 5 DSC thermograms of neat PVA (a) and PVA/Au nanocomposites with 1.0 and 5.3 wt % of inorganic phase (b and c, respectively) in nitrogen atmosphere.

the band peaking at 1329 cm^{-1}. This band is the consequence of the coupling of O-H in plane vibration (strong line at 1420 cm^{-1}) with C—H wagging vibrations. The decrease in the intensity ratio between bands at 1420 and 1329 cm^{-1} with an increase in the content of nanofiller implies that decoupling process between mentioned vibrations takes place due to interaction between Au NPs and the OH groups from the PVA chains.[13,26] These results indicate that main interaction between surface of Au NPs and PVA chains occurs over O-H groups.

In addition, FTIR spectra of PVA/Au nanocomposites revealed disappearance of the band positioned around 1570 cm^{-1}. According to Krimm et al.,[27] the PVA may contain some C=O groups within the chain, assigned to β-diketone groups. These authors suggested that position of this band should be at 1590 cm^{-1}. Our decision to assign band at 1570 cm^{-1} to β-diketone groups, probably in enol form, was supported by the presence of band at 1713 cm^{-1} associated to the stretching vibration of C=O functionality, which is verification of existence of residual vinyl acetate groups in partially hydrolyzed PVA.[28] Taking into account the presence of OH groups on the surface of Au nanocrystals, the possibility for hydrogen bond formation between them and β-diketone groups from PVA chain can be explanation for decrease in intensity and disappearance of band at 1570 cm^{-1}.

Moreover, the change of the band at 1141 cm^{-1}, corresponding to a symmetric C—C stretching mode in the crystalline regions of PVA matrix, was observed.[29] Upon incorporation of the Au NPs in the PVA matrix, small decrease in the intensity of this band indicates the decrease of the content of ordered/crystalline phase of the polymer. The presence of peaks at 917 cm^{-1} in all samples reveals the existence of syndiotactic structure in polymer chains.[30]

The heat resistance of nanocomposite and the stability of supermolecular structure of polymer in the system can be affected by the interaction between nanofiller and polymer matrix. The changes of the specific heat capacity of PVA matrix upon incorporation of Au NPs were investigated by DSC measurements in nitrogen atmosphere, and obtained results are shown in Figure 5. In the temperature range from 50 to about 140°C the broad endothermic peak was observed for all samples due to elimination of free and the hydrogen bonded water.[31] Sharp peak at 220°C corresponds to the melting of crystalline phase. It is important to notice that melting temperature (T_m) of the neat PVA is higher when compared with the T_m values of the PVA/Au nanocomposites. Also, the T_m of the PVA/Au nanocomposites decreases with the increase of the content of inorganic phase (almost 20°C for the highest concentration of Au NPs). The decrease of the T_m of semicrystalline polymers can be explained by the decrease of width and thickness of the lamellae during the crystallization process. The T_m of semicrystalline polymers is given by well-known equation[29]:

$$T_m = T_m^0\left[1 - \frac{2}{\Delta H^0}\left(\frac{\sigma_f}{L} + \frac{2\sigma_s}{D}\right)\right] \quad (4)$$

where T_m^0 is the equilibrium melting temperature of an infinitely thick crystal, ΔH^0 is enthalpy of melting, σ_f and σ_s are crystal surface free energies per unit area of fold surface and side surface, respectively, while L and D are thickness and width of the lamellae, respectively. PVA crystals are formed by the folding of polymer chains, which are arranging themselves parallel to each other. The adsorption of polymer chains onto the NPs decreases the mobility of chain segments as well as crystal perfection, and consequently the heat resistance of nanocomposite. In parallel, changes of T_m can be affected by the changes of the entropy of melt induced by the presence of NPs. According to the equation for the thermodynamic melting temperature ($T_m = \Delta H^0/(\Delta S_m - \Delta S_c)$ where ΔS_m is the entropy of melt and ΔS_c is the entropy of crystal phase), anchoring of polymer segments onto the NPs can cause decrease of the melt entropy due to configuration constrains, thus increasing the T_m. In other words, the measured T_m depends on the relative ratio between the changes of lamellae dimensions and entropy of melt induced by the nanofiller.

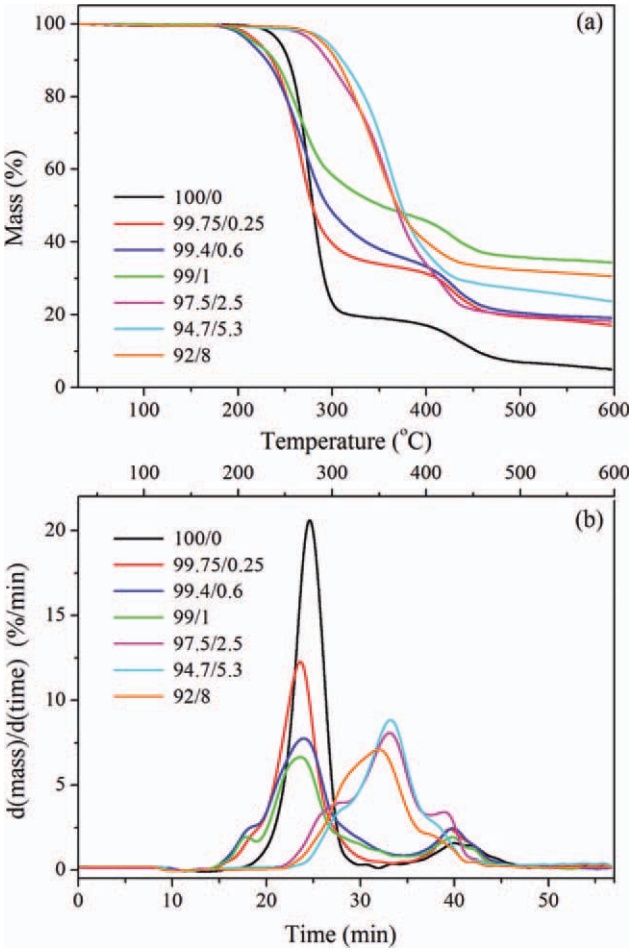

Figure 6 TG (a) and DTG (b) curves of dynamic thermal degradation of PVA and PVA/Au nanocomposites in nitrogen atmosphere. [Color figure can be viewed in the online issue, which is available at wileyonlinelibrary.com.]

Influence of Au NPs on the thermal stability of the PVA matrix was investigated using thermogravimetric measurements (see Fig. 6). The thermal degradation of neat PVA as well as PVA/Au nanocomposites with low content of nanofiller (≤1 wt %) can be roughly regarded as a two-step degradation process, while the degradation of nanocomposites with higher content of inorganic phase practically occurs in one step. In addition, incorporation of small amounts of Au NPs slightly decreased thermal stability of polymer matrix, while the higher concentration of nanofiller shifted the degradation process to higher temperatures, indicating improvement of thermal stability of nanocomposites in comparison with the neat PVA.

Two characteristic temperatures can be derived from TG and DTG curves: (i) the temperature of the degradation onset (T_{onset}), and (ii) the temperature of the maximum degradation rate (T_{max}). These characteristic temperatures as a function of the content of inorganic phase are shown in Figure 7. Nonlinear dependencies of these characteristic temperatures

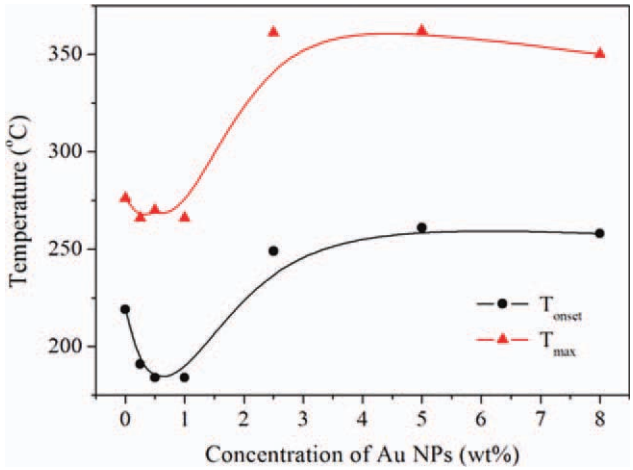

Figure 7 Temperature of degradation onset (T_{onset}) and temperature at the maximum degradation rate (T_{max}) as a function of the content of inorganic phase. [Color figure can be viewed in the online issue, which is available at wileyonlinelibrary.com.]

indicated the difference in the degradation process between the neat PVA and PVA/Au nanocomposites, as well as between the nanocomposites with low and high concentration of Au NPs. In addition, the dependence of the weight residue on the content of inorganic phase is presented in Figure 8. It should be noticed that thermal degradations of PVA/Au nanocomposites were completed with the larger amount of residue compared with that of the neat PVA. This effect is especially pronounced for the low loading of nanofiller (≤1 wt %). It is important to point out that changes in the thermal degradation of PVA are solely the consequence of the presence of the NPs, because gamma-irradiation (in applied dose range) does not induce any change in the polymer.[32]

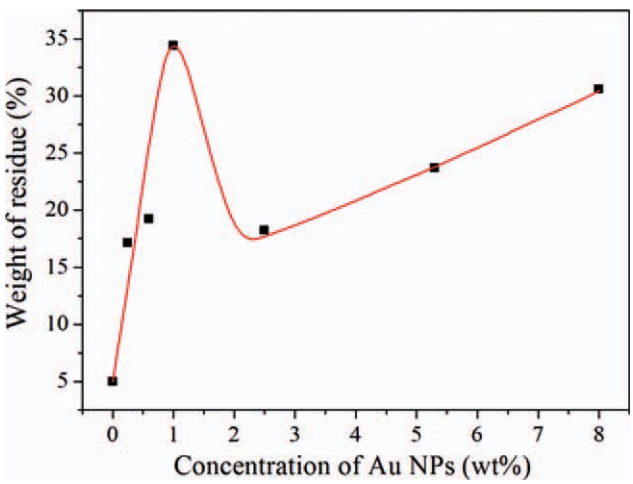

Figure 8 Weight of residue as a function of the content of inorganic phase. [Color figure can be viewed in the online issue, which is available at wileyonlinelibrary.com.]

The first degradation step of neat PVA involves the chain-stripping elimination reaction of H_2O followed by chain-scission reaction. The main decomposition products in this degradation step are conjugated and nonconjugated polyenes, as well as *cis*- and *trans*- allylic-methyls.[33,34] The second step of thermal degradation occurs at higher temperatures, and in this step, the degradation is dominated by the chain-scission reactions, side-reactions and cyclization reactions (Diels–Alder intra- and intermolecular cyclization followed by dehydrogenation with aromatization). The degradation products are acetaldehyde, acetic acid, polyenes, benzenoid derivatives, and a small amount of furan.[35]

The difference between degradation mechanism of the nanocomposites with low content of inorganic phase and the neat PVA is the presence of the side peak at the lower temperature in the first degradation step [Fig. 6(b)]. This peak can be caused by the elimination reactions, while the main peak appears due to the overlap of the continual eliminations and chain-scission reactions which need more energy and occur at a higher temperature.[33,34] In the second degradation step of nanocomposites chain-scission, cyclization, and radical reaction pathways, which occur in parallel, are responsible for the conversion of unsaturated hydrocarbons into substituted aromatic or aliphatic hydrocarbons.

The improved thermal stability upon incorporation of Au NPs with content of inorganic phase higher than 1 wt % can be explained by a barrier model. This model suggests that a build up of polymeric-inorganic char on the surface of the polymer melt provides a barrier for mass and heat transfer. Retardation of thermal degradation was mainly due to suppression of the mobility of polymer chains by the NPs. Two general mechanisms are probably responsible for the modes of action of Au NPs on the thermal stability of PVA. One is described as a chemical constraint for the H_2O elimination due to the interaction of Au NPs with OH groups (confirmed by FTIR analysis), which may increase energy barrier of the chain-stripping elimination of H_2O and induce a shift of the thermal degradation of partial decomposition products toward chain-scission and formation of methyl terminated polyenes. The other mechanism is described as a physical constraint, i.e., reduced molecular mobility which induces decrease of their collision frequency and suppresses cyclization and chain transfer reactions. As a consequence, upon incorporation of higher content of Au NPs the thermal degradation toward chain-scission reactions becomes dominant, resulting in degradation of greater number of PVA molecules and giving the smaller weight of residue. On the other hand, upon incorporation of smaller content of Au NPs the extent of chemical and physical constraints is much less pronounced. In this case, the cyclization and chain transfer reactions becomes dominant and the weight residue of the thermal degradation was greater.[36,37]

CONCLUSIONS

The PVA/Au nanocomposites were prepared using the steady state gamma-irradiation for *in situ* radiolytic synthesis, followed by solvent evaporation. Uniform spherical Au NPs, with diameter smaller than 10 nm were obtained and homogeneously embedded in PVA matrix. The optical spectra of Au colloids as well as of PVA/Au nanocomposites show the presence of characteristic SPR band. These results are discussed in terms of the Mie theory for metal NPs and Maxwell-Garnett effective medium theory for nanocomposites. Calorimetric data revealed the decrease of heat resistance of PVA/Au nanocomposites compared with neat PVA. During crystallization process, the mobility of polymer chain segments decreases due to the absorption on the surface of NPs, and consequently leads to reduced crystal perfection. Nanocomposites dynamic thermal degradation takes place by a more complex pathways compared with the degradation of neat PVA. In this study, only the higher contents of nanofillller induce improvement of thermal stability of PVA/Au nanocomposites. Moreover, incorporation of higher quantities of Au NPs in PVA matrix leads to the disappearance of the first step of degradation suggesting the degradation via competitive reactions, chain-stripping elimination and chain-scission.

References

1. Kreibig, U.; Vollmer, M. Optical Properties of Metal Clusters, Springer Series in Materials Science; Springer: Berlin, 1995; Vol. 25.
2. Bohren, C. F.; Huffman, D. R. Absorption and Scattering of Light by Small Particles; Wiley: New York, 1983.
3. Kelly, K. L.; Coronado, E.; Zhao, L. L.; Schatz, G. C. J Phys Chem B 2003, 107, 668.
4. Mulvaney, P. Langmuir 1996, 12, 788.
5. Raveendran, P.; Fu, J; Wallen, S. L. Green Chem 2006, 8, 34.
6. Sau, T. K.; Pal, A.; Jana, N. R.; Wang, Z. L.; Pal, T. J Nanopart Res 2001, 3, 257.
7. Henglein, A. Langmuir 1999, 15, 6738.
8. Li, T.; Park, H. G.; Choi, S. H. Mater Chem Phys 2007, 105, 325.
9. Liu, T.; Tang, J.; Jiang, L. Biochem Biophys Res Commun 2002, 295, 14.
10. Prabaharan, M.; Grailer, J. J.; Pilla, S.; Steeber, D.A.; Gong, S. Biomaterials 2009, 30, 6065.
11. Rahman, W. N.; Bishara, N.; Ackerly, T.; He, C. F.; Jackson, P.; Wong, C.; Davidson, R.; Geso, M. Nanomed Nanotechnol Biol Med 2009, 5, 136.
12. Gachard, E.; Remita, H.; Khatouri, J.; Keita, B.; Nadjo, L.; Belloni, J. New J Chem 1998, 22, 1257.

13. Krklješ, A.; Nedeljković, J. M.; Kačarević-Popović, Z. M. Polym Bull 2007, 58, 271.
14. Tripathy, P.; Mishra, A.; Ram, S.; Fecht, H.-J.; Bansmann, J; Behm, R. J Nanotechnol 2009, 20, 075701.
15. Draganic, I. G.; Draganic, Z. D. The Radiation Chemistry of Water; Academic Press: New York, 1971.
16. Chang, C. P.; Tseng, C. C.; Ou, J. L.; Hwu, W. H.; Ger, M. D. Colloid Polym Sci 2010, 288, 395.
17. Mie, G. Ann Phys 1908, 25, 377.
18. Maxwell Garnett, J. C. Philos Trans R Soc London Ser A 1904, 203, 385.
19. Johnson, P. B.; Christy, R.W. Phys Rev B: Condens Matter 1972, 6, 4370.
20. Henglein, A. J Phys Chem 1993, 97, 5457.
21. Krklješ, A. N.; Marinović-Cincović, M. T.; Kačarević-Popović, Z. M.; Nedeljković, J. M. Eur Polym Mater 2007, 43, 2171.
22. Templeton, A. C.; Pietron, J. J.; Murray, R. W.; Mulvaney, P. J Phys Chem B 2000, 104, 564.
23. Božanić, D. K.; Djoković, V.; Blanuša, J.; Nair, P. S.; Georges, M. K.; Radhakrishnan, T. Eur Phys J E 2007, 22, 51.
24. Tadd, E.; Zeno, A.; Zubris, M.; Dan, N.; Tannenbaum, R. Macromolecules 2003, 36, 6497.
25. Coates, J. P. Encyclopedia of Analytical Chemistry; Wiley: Chichester, UK, 2000.
26. Bai, J.; Li, Y.; Yang, S.; Du, J.; Wang, S.; Zheng, J.; Wang, Y.; Yang, Q.; Chen, X.; Jing, X. Solid State Commun 2007, 141, 292.
27. Krimm, S.; Liang, C. Y.; Sutherland, G. B. B. M. J Polym Sci 1956, 22, 227.
28. Alexy, P.; Káchová, D.; Kršiak, M.; Bakoš, D.; Šimková, B. Polym Degrad Stab 2002, 78, 413.
29. Mallapragada, S. K.; Peppas, N. A. J Polym Sci Part B: Polym Phys 1996, 34, 1339.
30. Abdelaziz, M.; Ghannam, M. M. Phys B 2010, 405, 958.
31. Bandyopadhyay, A.; Bhowmick, A. K. Plast Rubber Compos 2006, 35, 210.
32. Chapiro, A. Radiation Chemistry of Polymeric Systems; Wiley: New York, 1962.
33. Alexy, P.; Bakos, D.; Crkonova, G.; Kolomaznik, K.; Krsiak, M. Macromol Symp 2001, 170, 41.
34. Gilman, J. W.; VanderHart, D. L.; Kashiwagi, T. Fire and Polymers II: Materials and Tests for Hazard Prevention; American Chemical Society: Washington, DC, 1994.
35. Peng, Z.; Kong, L. X. Polym Degrad Stab 2007, 92, 1061.
36. Krklješ, A. N.; Marinović-Cincović, M. T.; Kačarević-Popović, Z. M.; Nedeljković, J. M. Thermochim Acta 2007, 460, 28.
37. Peng, Z.; Kong, L. X.; Li, S. D.; Spiridonov, P. J Nanosci Nanotechnol 2006, 6, 3934.